PNAS RESEARCH ARTICLE | CELL BIOLOGY

α-lipoic acid ameliorates consequences of copper overload by up-regulating selenoproteins and decreasing redox misbalance

Ekaterina Kabin[a,b,1], Yixuan Dong[b,2], Shubhrajit Roy[b,2], Julia Smirnova[a], Joshua W. Smith[c], Martina Ralle[d], Kelly Summers[b], Haojun Yang[b], Som Dev[b], Yu Wang[b], Benjamin Devenney[b], Robert N. Cole[c], Peep Palumaa[a], and Svetlana Lutsenko[b,1]

Edited by Vadim Gladyshev, Harvard Medical School, Boston, Massachusetts; received April 13, 2023; accepted August 18, 2023

α-lipoic acid (LA) is an essential cofactor for mitochondrial dehydrogenases and is required for cell growth, metabolic fuel production, and antioxidant defense. In vitro, LA binds copper (Cu) with high affinity and as an endogenous membrane permeable metabolite could be advantageous in mitigating the consequences of Cu overload in human diseases. We tested this hypothesis in 3T3-L1 preadipocytes with inactivated Cu transporter Atp7a; these cells accumulate Cu and show morphologic changes and mitochondria impairment. Treatment with LA corrected the morphology of *Atp7a*$^{-/-}$ cells similar to the Cu chelator bathocuproinedisulfonate (BCS) and improved mitochondria function; however, the mechanisms of LA and BCS action were different. Unlike BCS, LA did not decrease intracellular Cu but instead increased selenium levels that were low in *Atp7a*$^{-/-}$ cells. Proteome analysis confirmed distinct cell responses to these compounds and identified upregulation of selenoproteins as the major effect of LA on preadipocytes. Upregulation of selenoproteins was associated with an improved GSH:GSSG ratio in cellular compartments, which was lowered by elevated Cu, and reversal of protein oxidation. Thus, LA diminishes toxic effects of elevated Cu by improving cellular redox environment. We also show that selenium levels are decreased in tissues of a Wilson disease animal model, especially in the liver, making LA an attractive candidate for supplemental treatment of this disease.

copper | α-lipoic acid | selenoprotein | oxidative stress | Wilson disease

Cu is an essential cofactor of enzymes participating in numerous biological processes ranging from cellular respiration to biosynthesis of neuromediators (1–4). Cu deficiency, observed in Menkes disease (MNK), is associated with lower activity of Cu-dependent enzymes, numerous metabolic abnormalities, and early death (4–8). MNK is caused by genetic mutations in ATP-driven Cu(I) transporter ATP7A. Inactivation of ATP7A results in the entrapment of dietary Cu in enterocytes, impaired Cu export from the intestine to the rest of the body, and systemic Cu deficit. Despite Cu deficiency, MNK patients exhibit paradoxical Cu accumulation in kidneys (9, 10), which worsens with Cu supplementation therapy and complicates patients' treatment. In another disorder of Cu homeostasis, Wilson disease (WD), mutations in the Cu(I) transporter ATP7B disrupt Cu export from the liver, disabling the major route of Cu removal from the body. WD patients suffer from Cu accumulation in tissues, especially in the liver and the brain, which causes oxidative stress, mitochondrial and metabolic dysfunction, and hepatic, neurologic, and behavioral pathologies (8, 11–14). WD is managed using Cu chelation therapy, supportive treatment with zinc salts, and low-Cu diets (4, 5, 11). The most frequently used Cu-chelators D-penicillamine (PA) and trientine (TR) (12, 15), while beneficial, have very slow response times and side effects, including neurological worsening (12, 16–18). Thiomolybdate salts have milder side effects and a faster response time (30 d), but their long-term safety and efficiency are still being investigated (15, 19, 20).

The need for safe and fast means of diminishing Cu toxicity stimulates search for new alternatives. A recent in vitro study found that alpha-lipoic acid (LA) binds Cu(I) ions with higher affinity than PA and TR (21). Lipoic acid, also known as thioctic acid, is an endogenously produced short fatty acid. It contains two sulfhydryl groups that can participate in redox reactions and also bind Cu(I) ions (21–24). LA is synthesized de novo from octanoic acid in mitochondria and serves as a cofactor for at least five dehydrogenase complexes (24–26). LA is already used for the treatment of diabetic neuropathy and is available as a dietary supplement (24, 27). Significantly, LA can pass through the blood–brain barrier—in contrast to PA or TR (27, 28). Consequently, we tested whether LA has beneficial effects in a cellular model of Cu overload and investigated the mechanisms of LA action and relevance of our findings to WD.

Significance

Copper is an essential biometal; however, Cu overload causes oxidative stress and debilitating pathologies, such as Wilson disease (WD). Renal Cu toxicity is observed in Menkes disease, and changing copper levels are seen in other neurologic disorders and aging. Copper chelators provide health benefits but have shortcomings, including limited permeability through brain barriers. We demonstrate that a natural metabolite—α-lipoic acid (LA)—decreases Cu toxicity similarly to chelation but acts through a different mechanism. While Cu chelators limit available Cu, LA boosts antioxidant defense by increasing levels of selenium and selenoproteins. Our finding that selenium is low in tissues of the WD animal model suggests that LA may have therapeutic value for WD, especially given its favorable safety profile.

Author contributions: E.K., J.S., J.W.S., K.S., R.N.C., P.P., and S.L. designed research; E.K., Y.D., S.R., J.S., J.W.S., M.R., K.S., and Y.W. performed research; H.Y., S.D., B.D., and R.N.C. contributed new reagents/analytic tools; E.K., Y.D., J.S., J.W.S., M.R., K.S., Y.W., P.P., and S.L. analyzed data; S.R., K.S., H.Y., S.D., and Y.W. read and commented on the manuscript; B.D. was involved in animal husbandry, read and commented on the manuscript; and E.K., Y.D., P.P., and S.L. wrote the paper.

The authors declare no competing interest.

This article is a PNAS Direct Submission.

[1]To whom correspondence may be addressed. Email: katjake.g@gmail.com or lutsenko@jhmi.edu.

[2]Y.D. and S.R. contributed equally to this work.

This article contains supporting information online at https://www.pnas.org/lookup/suppl/doi:10.1073/pnas.2305961120/-/DCSupplemental.

Published September 26, 2023.

Results

Elevated Cu Induces Morphological Changes in *Atp7a*$^{-/-}$ 3T3-L1 Cells. To determine whether LA ameliorates consequences of Cu overload, we used *Atp7a*$^{-/-}$-3T3-L1 cells (29), further referred to as KO. These cells lack Cu-transporter Atp7a and thus are unable to export Cu, which causes intracellular Cu accumulation (*SI Appendix*, Fig. S1 *A*–*F*). Nondifferentiated cells were used because LA inhibits differentiation of adipocytes (30–32). The obvious difference between control and KO cells is their morphology. Nondifferentiated 3T3-L1 preadipocytes can be either elongated or flattened (Fig. 1*A*), whereas KO cells are uniformly flattened and enlarged (Fig. 1*B*). Treatment with the Cu chelator BCS linked these morphological changes to cellular Cu content. Short-term treatment (24 to 48 h) did not significantly change cellular Cu and did not affect KO morphology (Fig. 1 *C*–*F* and *SI Appendix*, Fig. S2 and Table S1). After 10 d of treatment, Cu levels decreased significantly and were closer to that of WT (4.03 ± 0.86 fg Cu/cell and 3.14 ± 0.49 fg Cu/cell, respectively, Fig. 1 *C* and *G*) Similarly, the fraction of flattened KO cells decreased to 61.3 ± 4.0 % and was close to that of WT (51.9% ± 9%, Fig. 1*D* and *SI Appendix*, Fig. S2 and Table S1). By day 17, Cu levels in the BCS-treated KO cells returned to nontreated WT levels and, morphologically, KO cells were indistinguishable from WT (Fig. 1 *D* and *E* and *SI Appendix*, Fig. S2). The majority of nontreated KO cells (87.1 ± 3.0%) remained enlarged and flattened (Fig. 1 *D*–*G* and *SI Appendix*, Fig. S2 and Table S1). The need for a long treatment time can be ascribed to BCS being membrane impermeable and only limiting Cu entry into cell, instead of sequestering intracellular Cu or facilitating Cu efflux.

Lipoic Acid Corrects *Atp7a*$^{-/-}$ Cell Morphology without Changing Cellular Cu Content. Treatment with LA, which is membrane permeable, did not improve cell morphology after 24- or 48-h treatment (Fig. 1 *D* and *F* and *SI Appendix*, Fig. S2 and Table S1). However, after 10 d, about 60% of cells treated with 5 μM LA were no longer enlarged (Fig. 1*D* and *SI Appendix*, Fig. S2 and Table S1) similarly to BCS-treated cells. After 17 d of treatment with either 5 μM or 25 μM LA, KO cells looked like WT (Fig. 1 *D* and *E* and *SI Appendix*, Fig. S2 and Table S1). Morphometric analysis confirmed that the decrease in cell area accompanied changes in cell shape (Fig. 1 *F* and *G*) and occurred at all LA concentrations (*SI Appendix*, Fig. S2). As the major changes in KO cell phenotype require 10 d of treatment with either reagent, most of the further analyses were completed at this time point.

While LA corrects morphology of KO cells at concentrations and with kinetics similar to BCS, further studies found marked differences in the BCS and LA mechanisms of action. In contrast to BCS, LA did not decrease cellular Cu content at all tested LA concentrations (Fig. 2*A* and *SI Appendix*, Fig. S3 *A* and *B*). To determine whether LA chelates Cu intracellularly, we examined the effect of LA on localization of Atp7a in WT cells. Atp7a localization is sensitive to cytosolic Cu levels: under low Cu, Atp7a is targeted to the *trans*-Golgi network (TGN), whereas elevated Cu triggers Atp7a trafficking from the TGN to vesicles (33, 34). In BCS-treated 3T3-L1 cells, Atp7a had expected perinuclear localization, consistent with the TGN targeting (Fig. 2*B* and *SI Appendix*, Fig. S4). In contrast, in cells treated with LA, Atp7a localized to vesicles (Fig. 2*B* and *SI Appendix*, Fig. S4), resembling the Atp7a response to Cu elevation (*SI Appendix*, Fig. S4). This result argued against LA chelating Cu and limiting its availability. To verify this conclusion, we characterized Cu speciation in cells using size-exclusion chromatography coupled to inductively coupled plasma mass spectrometry (ICP-MS). Analysis of homogenates of *Atp7a*$^{-/-}$ cells treated with or without LA demonstrated that, as expected, LA did not decrease Cu content in *Atp7a*$^{-/-}$ cells and that the vast majority of excess copper was in a protein-containing fraction and not in the low-molecular-weight fraction (Fig. 2 *C* and *D* and *SI Appendix*, Fig. S5).

We also considered the possibility that LA limits Cu availability in the cytosol by redistributing Cu to other compartments. To examine this possibility, we took advantage of the fact that the expression of cytosolic Cu(I)-binding proteins, metallothioneins MT-1 and MT-2, is up-regulated by elevated cytosolic Cu (34–38). Indeed, the *Mt-1* and *Mt-2* mRNA levels were higher in KO cells compared to WT (Fig. 2*E* and *SI Appendix*, Fig. S6). Treatment with BCS for 10 d, which lowered Cu content (Fig. 2*A*), decreased the *Mt-1* mRNA levels, whereas treatment with LA did not (Fig. 2 *F* and *G*). Upregulation of *Mt-2* mRNA was decreased by LA treatment but remained higher than the WT levels (*SI Appendix*, Fig. S6), providing evidence for differences in Mt-1 and Mt-2 regulation, previously reported for Zn (39). Taken together, the data provided compelling evidence that LA improves *Atp7a*$^{-/-}$ cells' phenotype by mechanisms other than limiting Cu availability. If LA does not chelate or redistribute Cu, then how does LA ameliorate Cu effects?

LA Increases Abundance of Selenoproteins. To better understand how LA affects KO cells, we compared changes in proteomes of KO cells treated with 10 μM BCS or 5 μM LA for 10 d using tandem mass tag (TMT) labeling and mass spectrometry. In nontreated KO cells, 167 proteins were up-regulated and 191 down-regulated (fold change $\log_2 > 0.5$, *P*-value 0.05; *SI Appendix*, Fig. S7*A*) compared to WT; these proteins participate in cellular metabolism, signaling, cell adhesion, and morphology (*SI Appendix*, Table S2). BCS treatment significantly changed proteins involved in metals metabolism and transport: Mt-1, Zn transporter Slc30a1, and Cu transporter Slc31a2 (Ctr2) were down-regulated, and Cu chaperone for superoxide dismutase (Ccs) was up-regulated (Fig. 3*A* and *SI Appendix*, Fig. S8 and Tables S3 and S4) in agreement with the decrease in cellular Cu content.

Cellular response to LA was completely different. The most significant change in the LA-treated KO cells (both fold change and p-value) was upregulation of selenoproteins. Out of 13 selenoproteins detected in our mass-spectrometry dataset, eight showed increased abundance after treatment with LA, including glutathione peroxidase 1 (Gpx1), phospholipid hydroperoxide glutathione peroxidase also known as glutathione peroxidase 4 (Gpx4), selenoprotein H (SelenoH), selenoprotein N (SelenoN), selenoprotein S (SelenoS), selenoprotein T (SelenoT), and selenoprotein W (SelenoW) (Fig. 3*B* and *SI Appendix*, Table S3). We verified the LA-dependent increase in selenoproteins by performing size-exclusion ICP-MS, which demonstrated not only a significant increase in the Se levels but also a predominant association of Se with the high-molecular-weight (protein) fraction (Fig. 3 *C* and *D*). In WT cells, treatment with LA also increased the abundance of selenoproteins Gpx1, SelenoH, SelenoW, and selenoprotein N (SelenoN) (*SI Appendix*, Fig. S7*B*).

LA Specifically Increases Cellular Selenium. To determine whether LA regulates expression of selenoproteins at the transcriptional level, we performed RT-qPCR analysis of mRNA levels and did not find a strong correlation between the levels of selenoproteins and their respective mRNA with or without LA treatment (Fig. 3 *E* and *F* and *SI Appendix*, Fig. S9). For most selenoprotein transcripts, the increase after LA treatment was either small (1.1 to 1.3 fold) or not observed, suggesting that the LA-induced increase of selenoproteins abundance is largely posttranscriptional. Cellular selenium levels are critical for selenoprotein synthesis because selenium should

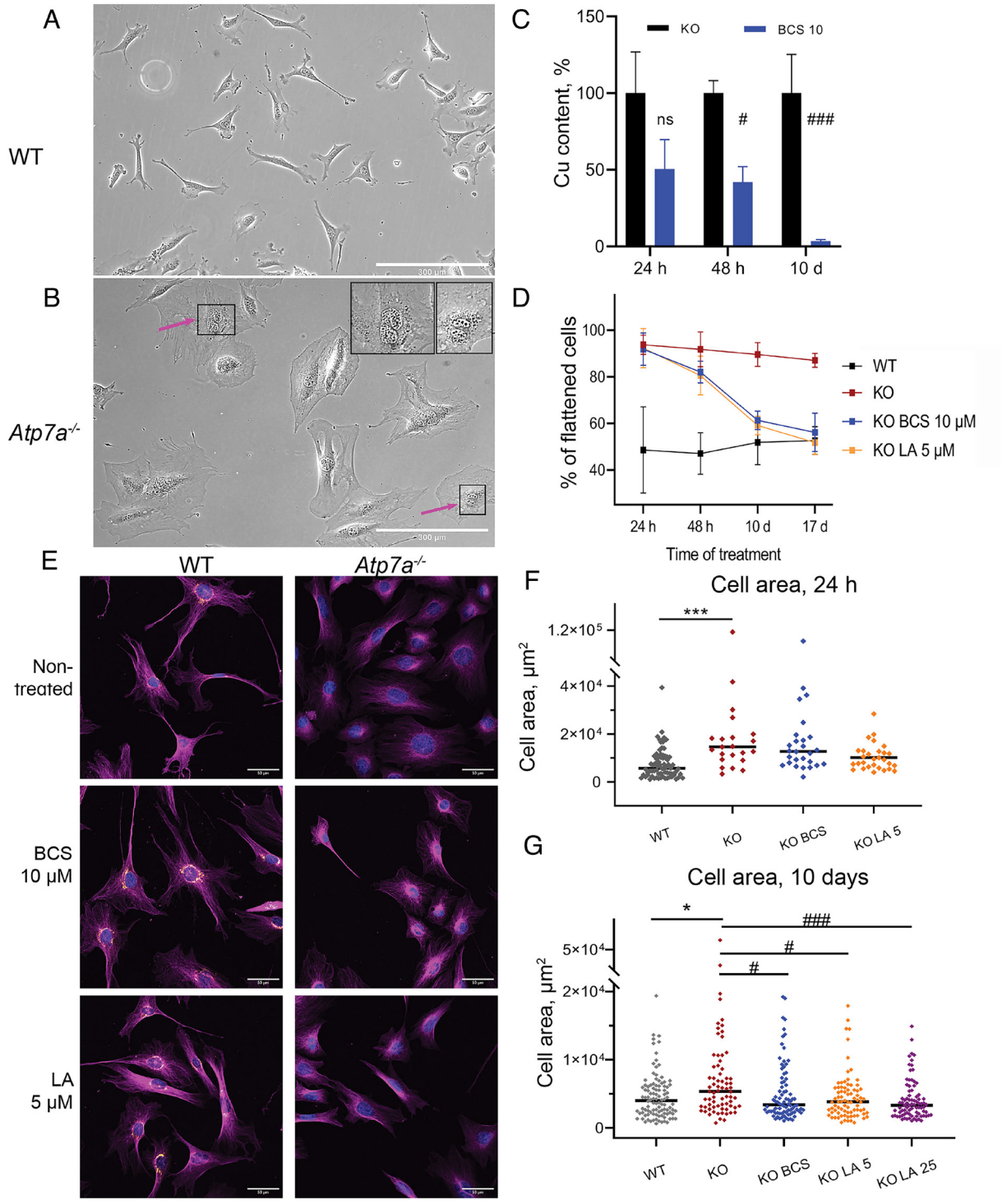

Fig. 1. α-lipoic acid reverses Cu-dependent changes in cell morphology of Atp7a-deficient preadipocytes. (*A*) Fibrillar morphology of WT preadipocytes and (*B*) flattened phenotype of KO cells; changes in nuclei size are indicated with arrows in the zoomed upper-right corner of the panel (scale bar, 300 µm). (*C*) Cellular Cu content in KO preadipocytes is decreasing during treatment with 10 µM BCS. (*D*) The number of flattened KO cells is decreasing during treatment with 10 µM BCS (blue) and 5 µM LA (orange) compared to nontreated conditions (dark-red). (*E*) Morphological changes in KO preadipocytes after 17 d of treatment with 10 µM BCS or 5 µM LA compared to the WT cell line visualized with immunostaining. Magenta α-tubulin, orange Atp7a (scale bar, 50 µm). Changes in cell area after 24 h (*F*) and 17 d (*G*) of treatment with BCS or LA. Each dot corresponds to an individual cell. The black line represents the median cell area. Cell areas were determined using ImageJ software. For panels (*C*, *F*, and *G*): comparison to nontreated WT cells designated with asterisks (*); comparison with the nontreated KO cells designated with sharp (#); *, # *P*-value < 0.05; ***, ### *P*-value < 0.001.

be available for incorporation into selenocysteine. As a result, abundance of selenoproteins often correlates with the cellular selenium content (40–43). We hypothesized that Se availability is low in the KO cells and that LA increases Se levels and selenoprotein synthesis. ICP-MS analysis confirmed that intracellular Se in KO cells was significantly lower than in WT cells (0.53 ± 0.03 fg/cell and 0.89 ± 0.09 fg/cell, respectively, Fig. 3*G*). BCS did not change Se content in either WT or in KO cells in agreement with the data on selenoprotein abundance (Fig. 3 *A* and *E*–*G* and *SI Appendix*, Fig. S9 and Table S3). In contrast, LA increased Se levels in both WT and KO cells in a dose-dependent manner. In KO cells treated with higher concentrations of LA (25 and 100 µM), Se content

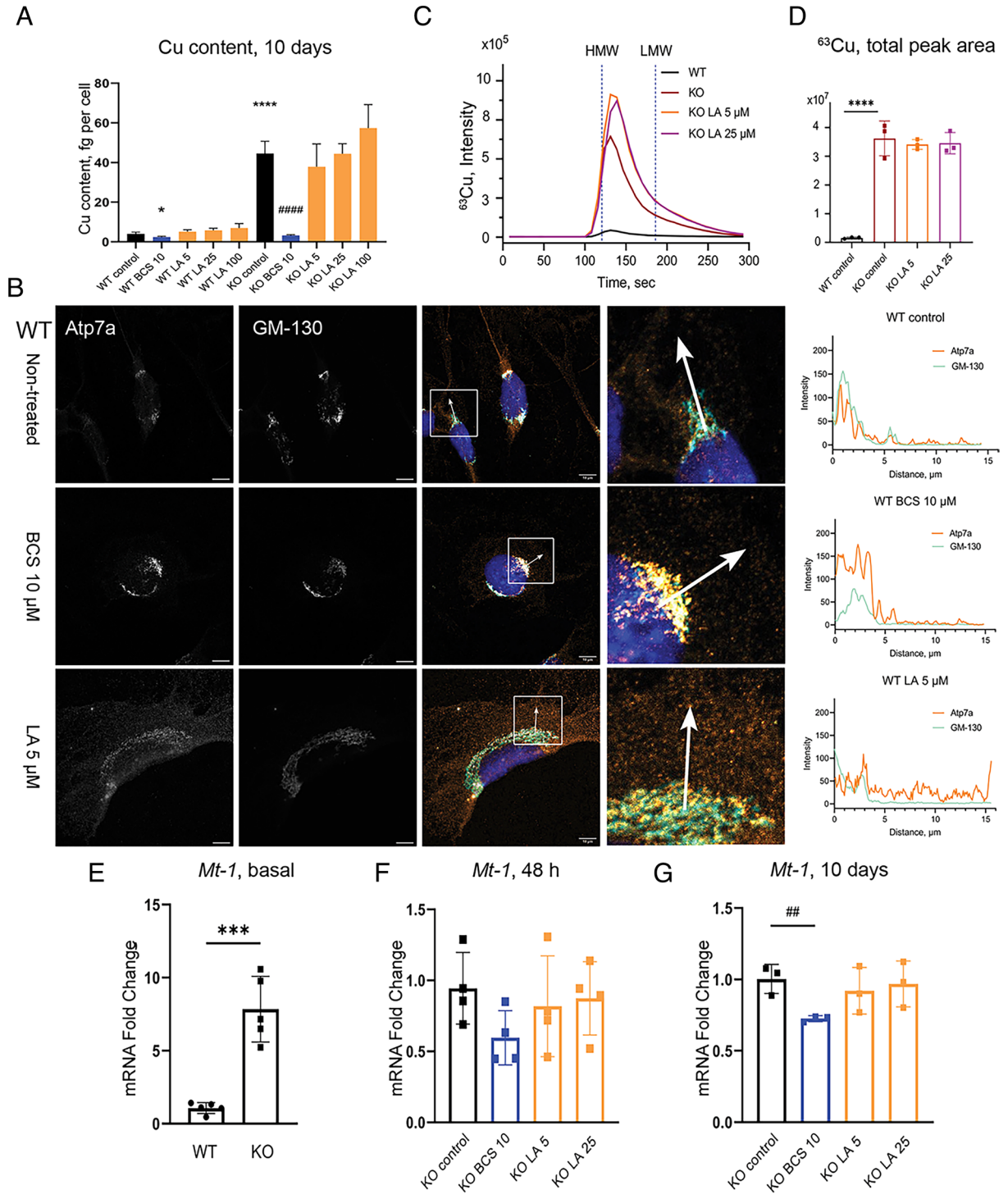

Fig. 2. LA does not alter cellular Cu content and causes relocalization of Atp7a in 3T3-L1 cells. (*A*) Cu content in WT and KO preadipocytes after 10 d of treatment with 10 µM BCS or different concentrations of LA. (*B*) Localization of Atp7a in 3T3-L1 WT cells after 10 d of treatment with 10 µM BCS or 5 µM LA. Orange Atp7a, cyan GM-130 (scale bar, 10 µm). Differences in the localization pattern of Atp7a and GM-130 are shown in white squares. Colocalization of Atp7a and GM-130 is quantified using ImageJ and visualized in GraphPad Prism. (*C*) Average chromatogram (n = 3 per group) of ^{63}Cu species in cell lysates of 3T3-L1 KO preadipocytes after 10 d of treatment with different concentrations of LA and (*D*) quantification of total ^{63}Cu peak areas normalized by ^{133}Cs signal and protein content (mean ± SD, n = 3). Nontreated WT and KO cells were used as respective controls. Vertical blue dashed lines (120.8 s and 186 s) indicate the retention time of high- and low-molecular-weight species (HMW and LMW, correspondingly) based on retention time of CuHSA (M ≈ 66 kDa) and Cu-EDTA (Mw 355.8 Da), respectively (*SI Appendix*, Fig. S5). (*E*) Relative expression of *Mt-1* in WT and KO preadipocytes on day 0 (n = 5), (*F*) after 48 h (n =4), and (*G*) after 10 d (n=3) of treatment with BCS or LA. For panels (*A*, *D*, *E*, and *G*): *P*-values for WT cells shown with asterisks (*) and for KO cells with sharp (#); * – *P*-value < 0.05; ## – *P*-value < 0.01; ***, ### – *P*-value < 0.001; **** – *P*-value < 0.0001.

(0.82 ± 0.04 fg/cell and 0.98 ± 0.05 fg/cell, Fig. 3*G*) became similar to that in nontreated WT cells (0.89 ± 0.09 fg/cell, Fig. 3*G*).

To test whether the effect of LA was specific to Se, we measured Fe, Zn, and Mn in control and KO cell lines after 24 h, 48 h, and 10 d of treatment. Fe levels were unchanged by Cu accumulation, and neither LA nor BCS altered Fe content in either WT or KO cells (*SI Appendix*, Figs. S10 *A* and *B* and S11*A*). Zn was approximately 25% higher in KO cells compared to WT (*SI Appendix*,

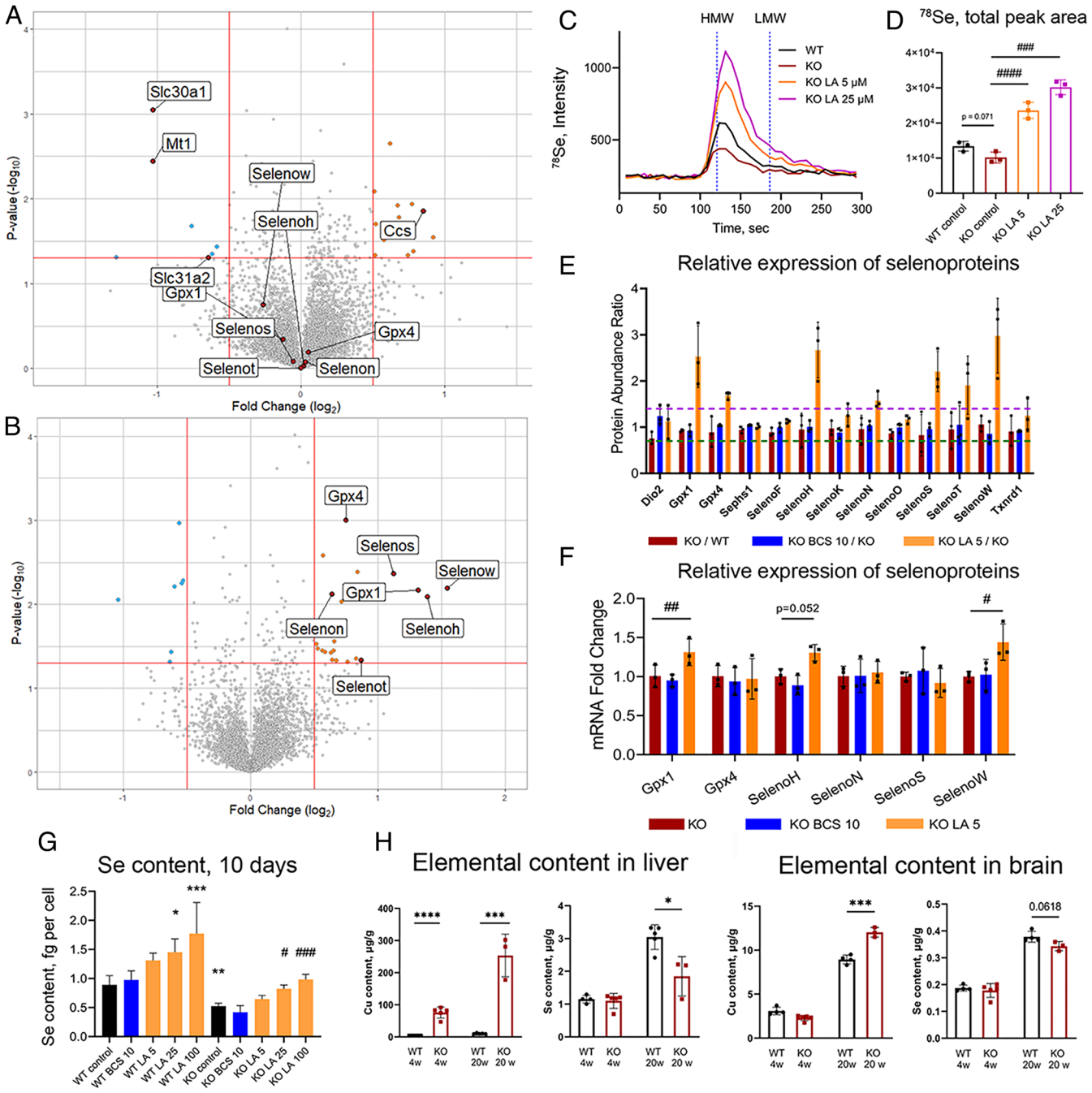

Fig. 3. LA up-regulates selenoproteins and increases cellular Se content. (*A*) Volcano plot comparing proteome of KO cells treated with 10 µM BCS for 10 d to nontreated KO cells and (*B*) KO cells treated with 5 µM LA for 10 d to nontreated KO cells. (*C*) Average chromatogram (n = 3 per group) of ^{78}Se species in cell lysates of KO preadipocytes after 10 d of treatment with different concentrations of LA and (*D*) quantification of total ^{78}Se peak areas normalized by ^{133}Cs signal and by protein content (data present as mean ± SD, n = 3). Nontreated WT and KO cells are used as controls. Vertical dashed lines (120.8 s and 186 s) demonstrate retention time of high- and low-molecular-weight species (HMW and LMW, correspondingly) based on retention time of CuHSA (Mw ≈ 66 kDa) and Cu-EDTA (Mw 355.8 Da), correspondingly (*SI Appendix*, Fig. S5). (*E*) Relative abundances of all selenoproteins identified by TMT labeling mass spectrometry in WT and KO preadipocytes after 10 d of treatment with 10 µM BCS or 5 µM LA (n = 3). The horizontal dashed lines at 1.4 (purple) and 0.7 (dark-green) indicate cutoff values for significant changes in protein abundance (upregulation and downregulation, correspondingly). (*F*) The mRNA for selenoproteins in KO cells relative to WT without treatment and after 10 d of treatment with 10 µM BCS or 5 µM LA (n = 3). For more details, see *SI Appendix*, Figs. S9 and S10. (*G*) Selenium content in WT and KO preadipocytes after 10 d of treatment with 10 µM BCS or different concentrations of LA. (*H*) Cu and Se content in the liver and brain tissue of 4- and 20-wk-old WT and *Atp7b*$^{-/-}$ mice; the two-tailed *t*-test was used for pairwise statistical analysis. For panels (*D*–*G*): comparison to nontreated WT cells is indicated with asterisks (*) and comparison with nontreated KO cells with sharp (#). For panels (*F*–*I*): *, # – *P*-value < 0.05; **, ## – *P*-value < 0.01; ***, ### – *P*-value < 0.001; ****, #### – *P*-value < 0.0001.

Figs. S10 *C* and *D* and S11*B*), similar to findings in the mouse model of Wilson disease (44). BCS returned Zn levels to that of WT after 10 d of treatment (*SI Appendix*, Fig. S11*B*), whereas LA did not (*SI Appendix*, Figs. S10*D* and S11*B*). Mn levels were significantly higher in KO cells compared to WT (*SI Appendix*, Figs. S10 *E* and *F* and S11*C*). After 10 d of treatment with either BCS or LA, Mn returned to the WT levels (*SI Appendix*, Figs. S10 *E* and *F* and S11*C*). Thus, increase in Se is specific to LA, whereas the effect on Mn is not.

***Atp7b*$^{-/-}$ Mice Have Decreased Selenium Content in The Liver and The Brain.** 3T3-L1 *Atp7a*$^{-/-}$ is a fibroblast model of Cu overload,

and whether Cu excess impacts Se content in vivo was unclear. To answer this question, we measured Se content in the liver and brain samples of *Atp7b*$^{-/-}$ mice, an animal model of Wilson disease (45), which accumulate Cu in tissues. In presymptomatic 4-wk-old *Atp7b*$^{-/-}$ mice, hepatic Se was not altered compared to the age-matched WT, even though Cu was elevated (Fig. 3*H*). At 20 wk, *Atp7b*$^{-/-}$ mice accumulated approximately three times more Cu in their livers compared to younger animals and had significantly decreased Se (Fig. 3*H*). A similar pattern was seen in the brain (Fig. 3*I*). In the heart, Se was markedly decreased even though Cu levels were comparable to WT (*SI Appendix*, Fig. S12*A*). Se content in the *Atp7b*$^{-/-}$ kidneys was not changed comparing to WT despite significantly elevated Cu (*SI Appendix*, Fig. S12*B*).

To determine whether low hepatic Se in *Atp7b*$^{-/-}$ mice reflects low levels of selenoproteins or their transcripts (or both), we took advantage of RNA sequencing and proteomics data for 20-wk-old *Atp7b*$^{-/-}$ mice that we generated previously (46, 47). These data demonstrated that out of 12 selenoproteins identified in the liver proteome, six showed significant downregulation (>1.5 fold, *P*-value < 0.05, *SI Appendix*, Table S5). This decrease was not due to the decreases in the selenoprotein transcripts: we detected mRNA for 20 out 25 selenoproteins, and most were either not changed or modestly up-regulated (*SI Appendix*, Table S5). Taken together, these results demonstrate that WD mice with a developed liver pathology, similarly to *Atp7a*$^{-/-}$ cells, have dysregulated selenium homeostasis, lower selenium, and diminished levels of several selenoproteins.

LA Protects Cu Overloaded Cells from Cu-Induced Redox Stress. Selenoproteins influence cellular redox balance by maintaining the ratio of reduced and oxidized glutathione (GSH:GSSG) and decreasing levels of peroxides (48, 49). We hypothesized that the LA-dependent increase in selenoproteins improves the antioxidant capacity of KO cells and diminishes oxidative stress caused by excess Cu. To test this hypothesis, we first used GRX1-roGFP2-based redox sensors targeted to different intracellular compartments (29, 50) and live cell measurements before and after treatments with LA for 10 d. Targeting of GRX1-roGFP2, MTS-GRX1-roGFP2, and NLLS-GRX1-roGFP2 to the cytosol, mitochondria, and nuclei, respectively, was verified by laser-scanning microscopy (*SI Appendix*, Fig. S13). As expected, nontreated KO cells show higher sensor oxidation in all three cellular compartments compared to nontreated WT cells (29) and (Fig. 4 *A*–*C*) treatment with LA significantly decreased sensor oxidation in the cytosol, mitochondria, and nuclei of KO cells, indicative of improved redox balance (Fig. 4 *A*–*C*).

To verify this conclusion, we examined protein oxidation in WT, KO, and KO cells treated with LA. We focused on the sulfur-containing amino acids, Cys and Met, because they are highly susceptible to oxidation, which can be prevented or reversed by other sulfur-containing molecules and/or by selenoproteins, such as methionine sulfoxide reductases MSRB1 (51). In total, there were 6,949 uniquely oxidized peptidoforms [i.e., unique peptides with specific modification(s)] across 2,271 proteins. To compare protein oxidation between the WT, KO, and KO+LA samples, we selected 2,400 peptidoforms that were found in all three groups and evaluated distribution of abundances of oxidized peptides normalized to total protein. This analysis demonstrated that the KO cells have significantly higher protein oxidation and that treatment with LA significantly decreases it (Fig. 4*D*). Initial evaluation of proteins undergoing LA-reversible oxidation found that these proteins are located in different cellular compartments and are involved in regulation of cytoskeleton assembly (Map6, Myo1c, Tagln2), chromosome maintenance and RNA processing (Eef2, Eif4g2, Mcm6), and mitochondria function (see examples in *SI Appendix*, Table S6).

To test whether the LA-dependent changes in redox balance and protein oxidation benefit cell functions, we measured mitochondria respiration using the Seahorse XF Cell Mito Stress Test (*SI Appendix*, Fig. S14*A*). The KO cells demonstrate a lower oxygen consumption rate (ref. 52 and *SI Appendix*, Fig. S14*B*) and lower spare respiratory capacity (Fig. 4*E*) than WT, consistent with increased mitochondria oxidation (Fig. 4*B*). After 48 h of treatment, both parameters were improved by either BCS or LA and became similar to WT cells (Fig. 4 *E* and *F* and *SI Appendix*, Fig. S14 *B* and *C*).

Finally, we examined whether the defects in mitochondria function in *Atp7a*$^{-/-}$ cells could be a result of a Cu-dependent loss of mitochondria protein lipoylation, as was observed in cancerous cells undergoing cuproptosis (53). However, western blot analysis of major lipoylated enzymes dihydrolipoamide S-acetyltransferase (Dlat) and dihydrolipoamide S-succinyltransferase (Dlst) found no difference in their abundance, arguing against LA altering this pathway in 3T3-L1 mouse fibroblasts (Fig. 4 *G*–*I*). Taken together, the data suggested that LA protects *Atp7a*$^{-/-}$ cells from Cu overload by diminishing Cu-induced oxidative stress.

Selenium alone Partially Replicates Effects of LA. Lipoic acid is an antioxidant on its own (54). Therefore, it was unclear whether the beneficial effects of LA are associated with LA increasing cellular Se content or via Se-independent antioxidant activity of LA. To distinguish between these possibilities, we compared the effects of a well-known antioxidant N-acetyl cysteine (NAC) and LA on *Atp7a*$^{-/-}$ cell morphology and mitochondria respiration after 10 d of treatment. NAC at 5 μM improved *Atp7a*$^{-/-}$ cells morphology, highlighting the importance of redox balance for cell shape and size. However, NAC was significantly less effective compared to LA and also had no effect on *Atp7a*$^{-/-}$ mitochondria respiration (Fig. 5 *A*–*C* and *SI Appendix*, Fig. S15). These data suggested that an increase of Se/selenoproteins abundance may be an important component of LA activity. To test this hypothesis, we treated cells with either 5 μM LA, or 1 μM Se in a form of selenite, or both 1 μM Se and 5 μM LA. Neither Se alone nor Se with LA decreased the cytosolic Cu as indicated by unchanged levels of *Mt-1* and *Ctr1* (Fig. 6 *A* and *B*). The *Mt-2* levels were decreased (*SI Appendix*, Fig. S6) but remained above the WT levels, suggesting that regulation of *Mt-2* was only partially dependent of Cu. Cell morphology was improved by treatment with either Se or LA (Fig. 6*C*), which produced similar results, and LA with Se treatment had strongest effect on cell morphology (Fig. 6 *C* and *D* and *SI Appendix*, Fig. S15). Thus, increased Se availability plays a significant role in improving morphology of *Atp7a*$^{-/-}$ cells. However, Se alone or in combination with LA did not improve mitochondrial respiratory function (Fig. 6*E* and *SI Appendix*, Fig. S16), pointing to an additional role of LA in mitochondria.

Discussion

Here, we show that the natural membrane permeable metabolite, α-lipoic acid, diminishes toxic effects of elevated Cu in a cellular model of Cu overload. The mechanism of LA action is distinct from that of Cu chelator BCS, which gradually reduces the intracellular Cu content in KO cells by limiting Cu availability. We show that LA does not prevent Cu entry into the cells, does not form intracellular small-molecular-weight complexes with Cu, and does not redistribute Cu away from the cytosol. Instead, LA improves cellular redox status and reverses protein oxidation while Cu is elevated. Using analysis of proteomes, treatments with either

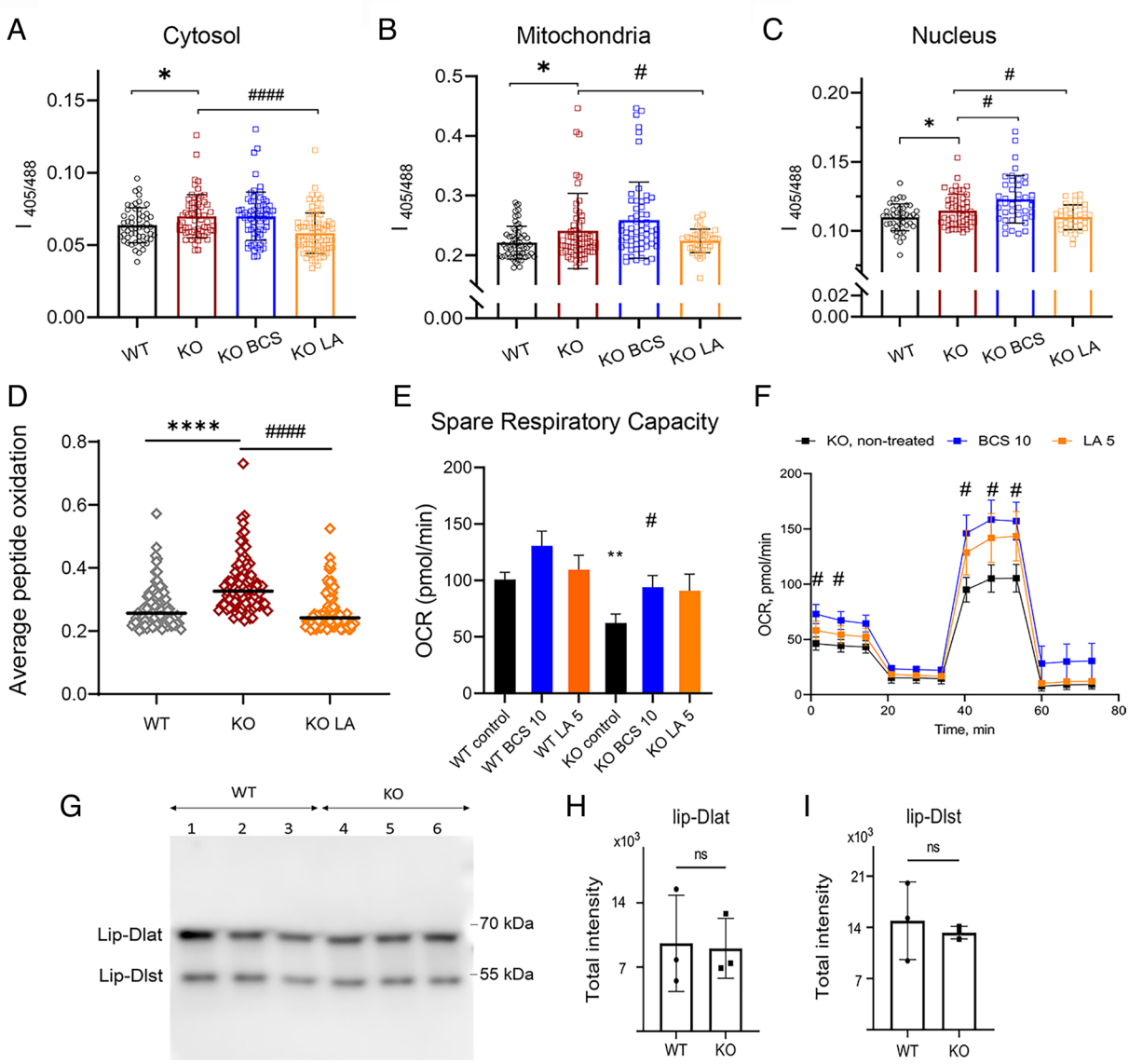

Fig. 4. Treatment with LA decreases redox misbalance in *Atp7a*$^{-/-}$ preadipocytes. Oxidation of the GRX-roGFP2 redox sensor in (*A*) cytosol, (*B*) mitochondria, and (*C*) nuclei of WT and KO preadipocytes after 10 d of treatment with 10 μM BCS or 5 μM LA (the number of cells in each group is > 40; n = 3). (*D*) Average oxidation of peptidoforms of WT and KO preadipocytes after 5 d of treatment with 5 μM LA estimated with quantitative redox proteomics. Peptides found in all treatment groups with a SD of mean less than 0.1 were selected for comparison. (*E*) Spare respiratory capacity (SRC) of WT and KO preadipocytes after 48 h treatment with 10 μM BCS or 5 μM LA. (*F*) Oxygen consumption rate (OCR) of KO preadipocytes after 48 h treatment with 10 μM BCS (blue) or 5 μM LA (orange) compared to nontreated KO cells (black). Data in *E* and (*F*) are mean ± SEM. (*G*) Representative western blot and (*H* and *I*) densitometric analysis of lipoylated proteins Dlat and Dlst in WT and KO cells. For panels (*A*–*F*): comparison with WT cells are shown with asterisks (*) and comparison with nontreated KO cells with sharps (#);*, # – *P*-value < 0.05; ** *P*-value < 0.01; ****, #### *P*-value < 0.0001.

Se or NAC and by evaluating Se species in the cells, we show that LA counteracts Cu-induced decrease of cells antioxidant capacity by increasing selenoprotein levels by increasing Se availability rather than altering transcription. Our data also suggest that in mitochondria, LA shows additional Se-independent activity.

BCS reverses changes in cellular Zn and Mn content and improves mitochondria respiratory function but does not increase Se, nor restore GSH:GSSG balance in either the cytosol or mitochondria, whereas LA does. This result suggests that oxidative stress in the KO cells is caused to a significant degree by a decrease in selenoproteins. In Wilson disease (in patients and animal models), antioxidant capacity is decreased, including a decrease in glutathione peroxidase (55). Given our finding that *Atp7b*$^{-/-}$ mice have lower Se levels in tissues, especially in the liver, it is tempting to speculate that treatment with LA could be a safe supplementary treatment that reduces oxidative stress, especially in the advanced disease. LA has already been tested in clinical trials for treatment of diabetic neuropathy (56) and neurodegenerative diseases (57), where it demonstrated a favorable safety profile at doses up to 1,800 mg/d (58). With administration of 600 mg of racemic LA, the maximum plasma concentrations of 6.86 ± 1.29 μg/mL (33 μM) could be reached (59). In our studies, we see improvements using 5 μM LA.

The LA-dependent increase in intracellular Se and upregulation of selenoproteins in WT and KO cells at concentrations as low as 5 μM is an unexpected effect of LA. Our data suggest that the most likely mechanism is facilitation of Se uptake, as we see more selenium with increasing LA concentration. How exactly LA increases Se uptake is still unknown. The apparent saturation of Se levels with higher LA concentrations and only small additive effect, when Se is combined with LA, point to a limiting step in this process, such as abundance/activity of a relevant transporter, which remains to be identified. Finally, by reversing protein oxidation of the RNA processing machinery, LA may facilitate

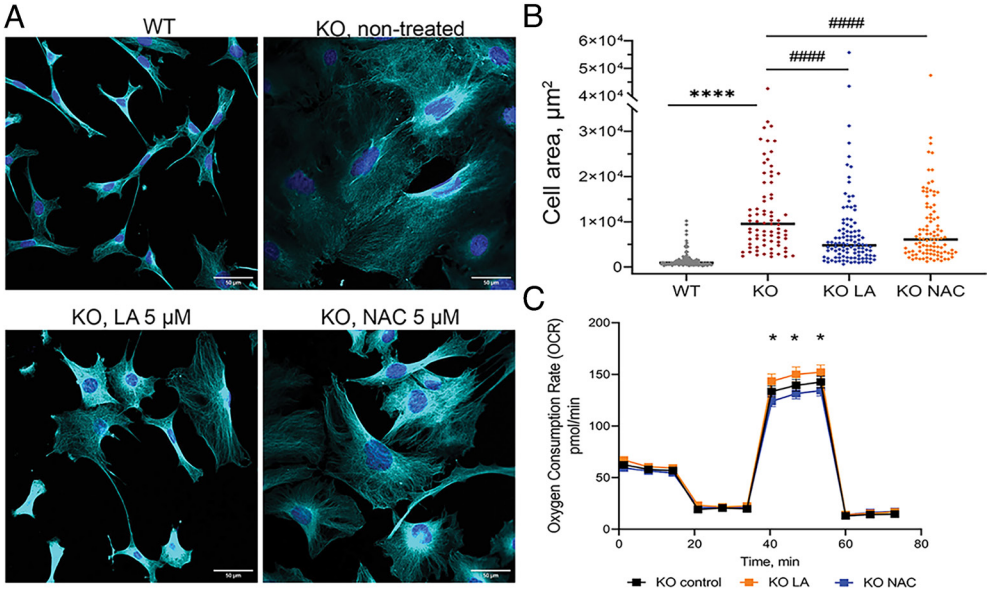

Fig. 5. NAC partially improves morphology but not mitochondrial respiration of *Atp7a*$^{-/-}$ preadipocytes. (*A*) Morphological changes in KO preadipocytes after 10 d of treatment with 5 μM LA or 5 μM NAC compared to nontreated KO and WT cell lines visualized with immunostaining. Cyan α-tubulin (scale bar, 50 μm). (*B*) Changes in cell area after 10 d of treatment with 5 μM LA or 5 μM NAC. Each dot corresponds to an individual cell. The black line represents the median cell area. Comparison to nontreated WT cells is designated with asterisks (*) and comparison with the nontreated KO cell line is designated with sharp (#). ****, #### – *P*-value < 0.0001. Cell areas were determined using ImageJ software. (*C*) Oxygen consumption rate (OCR) of KO cells treated with 5 μM LA (shown in orange) or 5 μM NAC (shown in blue) for 48 h compared to nontreated KO cells (shown in black). * – comparison of NAC-treated cells to LA-treated cells, * - *P*-value < 0.05.

protein synthesis of selenoproteins GPX4, SELENON, and SELENOS, which are less dependent on dietary Se (60, 61).

Cu negatively affects selenoprotein expression through a poorly understood mechanism not reversible by BCS (62), which is in agreement with our results. Selenoproteins play an essential role in protection of cells against oxidative stress. In WD mice, Se content is significantly lower in the liver, heart, and brain. In Se deficiency, the brain retains its Se content at the expense of other tissues (40). Therefore, diminished levels of Se and selenoproteins could be an important contributing factor to oxidative stress in WD, and LA may be beneficial as a supplementary treatment for WD. The ability of LA to improve cellular redox balance, decrease protein oxidation and restore cell morphology in the presence of elevated Cu supports this hypothesis. At the same time, our data do not exclude the possibility of minor changes in cellular Cu distribution contributing to improvement of cell phenotype. LA has relatively strong Cu(I)-binding affinity and some selenoproteins like SELENOH and SELENOW contain Cys-X-X-Sec motifs (63, 64), which are similar to Cys-X-X-Cys Cu-binding motifs. LA and selenoproteins can potentially bind excessive Cu(I) ions by these motifs into weak complexes and reduce Cu burden.

Lipoic acid improved mitochondrial respiratory function of *Atp7a*$^{-/-}$ cells, whereas neither Se alone nor NAC have beneficial effect on mitochondria. This result points to unique properties of LA that are necessary for this effect in mitochondria. Examination of protein lipoylation in mitochondria did not find significant effects on two major markers of this process, but more detailed evaluation is needed to better understand whether cuproptosis, ferroptosis, or other cell death mechanisms contribute to cells' response to Cu overload.

Previous studies found that Cu affects the structure of cytoskeletal proteins and their assembly into microtubules (65, 66). Oxidative stress affects the structure and dynamics of the cytoskeleton (67–70). Excess Cu can directly bind to Cys residues of cytoskeletal proteins or cause their oxidation, as we observed in our studies resulting in disrupted cytoskeleton arrangement and altered cellular morphology. We propose that BCS prevents unfavorable Cu binding to cytoskeletal proteins via Cu limitation and, therefore, restores the morphology of KO cells, and further estimation of Cu-binding affinities and protein competition experiments (21, 71) are needed to support this possibility. The LA-mediated protection of redox-sensitive Cys and Met residues of cytoskeletal proteins may have the same beneficial effect. Our study identified several cytoskeletal proteins protected from oxidation by LA treatment, and further studies will directly test the role of this reversible modification in the cytoskeletal proteins' function.

In summary, LA is a multifaceted player that diminishes the consequences of Cu overload and may serve as a supportive substance to chelation therapy, as it can restore cellular redox balance, protect proteome, and improve cellular functions.

Materials and Methods

Cell Morphology. 3T3-L1 preadipocytes were cultured in DMEM (Dulbecco's Modification of Eagle's Medium) with 4.5 g/L glucose, L-glutamine, and sodium pyruvate (Corning Cellgro) supplemented with 10% heat-inactivated FBS (Sigma-Aldrich) and 1% Penstrep (Gibco). Cells were supplemented with fresh medium every 2 d and passaged after reaching 90% confluency. Both 3T3-L1 and 3T3-L1 *Atp7a*$^{-/-}$ preadipocytes were incubated with or without 5 μM, 25 μM, or 100 μM of lipoic acid (LA, Sigma-Aldrich, cat #62320-5G-F) for various periods of time as indicated in the text. Cells treated with 10 μM bathocuproinedisulfonic acid (BCS, Sigma-Aldrich) were used as a positive control for Cu chelation. Treatment with 1 μM sodium selenite (Na_2SeO_3, 214485, Sigma; referred to as Se or selenite), alone or in combination with 5 μM LA, or with 5 μM N-acetylcysteine (NAC, Sigma-Aldrich, A7250) for 10 d was used to assess the effect of alternative antioxidants on KO cell morphology. Freshly prepared chemical solutions were added to the cells every 2 d along with a fresh medium as described above. During treatment with LA and BCS, phase-contrast images (Olympus IX51) were taken every 24 h to monitor changes in cell morphology; phase-contrast cells for morphometric analysis after treatment with NAC, Se, or Se and LA combination were done on day 10 of treatment. Detailed cell morphology assessment is described in *SI Appendix, Supplementary Methods*.

Immunostaining. Control 3T3-L1 WT cell and *Atp7a*$^{-/-}$ cells were treated with or without one of the following: 5 μM, 25 μM LA, 10 μM BCS, or 20 μM $CuCl_2$ for several time points (24 h, 48 h, 10 d, or 17 d). At the end of each treatment, cells were transferred to poly-L-lysine (Sigma-Aldrich) or rat tail collagen (354236,

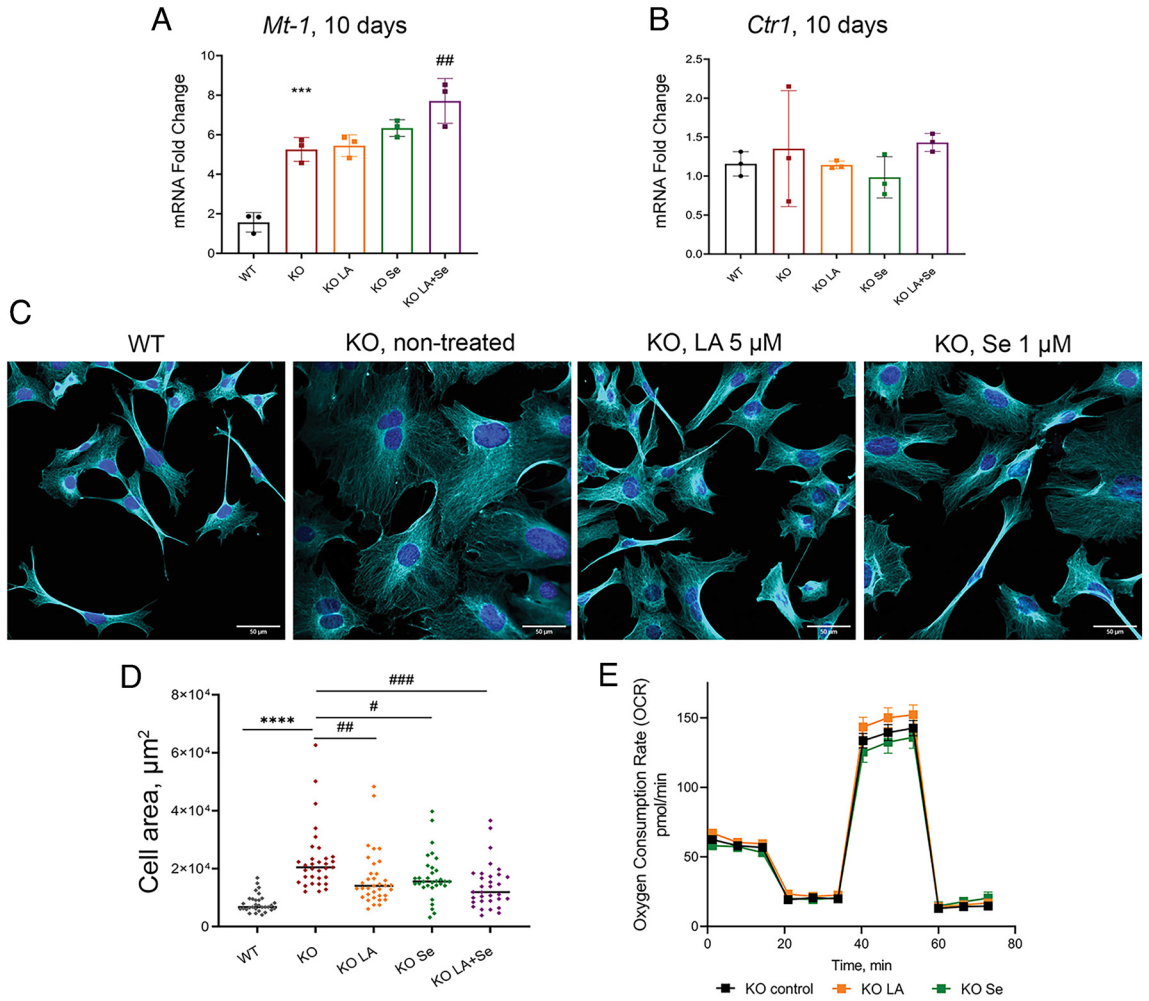

Fig. 6. Se improves morphology but not mitochondrial respiration of *Atp7a*$^{-/-}$ preadipocytes. (*A*) Relative expression of *Mt-1* and (*B*) *Ctr1* genes after 10 d of treatment with 5 μM LA or 1 μM Se, alone or in combination. (*C*) Morphological changes in KO preadipocytes after 10 d of treatment with 5 μM LA or 1 μM Se compared to nontreated KO and WT cell lines confirmed with immunostaining. Cyan α-tubulin (scale bar, 50 μm). (*D*) Changes in cell area after 10 d of treatment with 5 μM LA or 1 μM Se, alone or in combination. Each dot corresponds to an individual cell within the field of view. The black line represents the median cell area. Cell areas were determined using ImageJ software. (*E*) Oxygen consumption rate (OCR) of KO cells treated with 5 μM LA (shown in orange) or 1 μM Se (shown in dark-green) for 48 h compared to nontreated KO cells (shown in black). For panels (*A* and *D*): comparison to nontreated WT cells designated with asterisks (*); comparison with the nontreated KO cell line designated with sharp (#); # - *P*-value < 0.05; ## – *P*-value < 0.01; ***, ### – *P*-value < 0.001; **** – *P*-value < 0.0001.

Corning)–coated glass eight-chamber slides at a density of 0.7 × 10^4 cells/well. Further details are provided in *SI Appendix, Supplementary Methods*.

Immunoblot Analysis. Nontreated 3T3-L1 WT and *Atp7a*$^{-/-}$ cells were grown on 6-cm dishes. Details for the immunoblot experiment are provided in *SI Appendix, Supplementary Methods*.

TMT Labeling Mass Spectrometry, Peptide Identification, and Quantification. 3T3-L1 WT and *Atp7a*$^{-/-}$ preadipocytes were cultured in 60 mm dishes and treated with or without 5 μM LA or 10 μM BCS for 10 d. Cells were washed with ice-cold PBS, collected, and lysed with RIPA buffer with EDTA-free protease inhibitor cocktail on ice for 1 h and centrifuged at 3,000 *g* for 15 min. Protein concentration from the obtained lysate was estimated by the BCS assay. A mixture of 20 μg of total protein per well and 6× sample buffer were loaded to Laemmli SDS-PAGE gel and stained with Colloidal Blue staining (Thermo Fisher, LC6025) to confirm the quality of proteins. Protein lysate was further diluted to a concentration of 1 μg/μL. Then, proteins were reduced, alkylated, and precipitated in TCA/acetone mixture. Protein pellets were washed with ice-cold acetone, dried, and then reconstituted and proteolyzed. TMT labeling, peptide identification, quantification, and bioinformatics analysis are described in more details in *SI Appendix, Supplementary Methods*.

Biometals and Selenium Measurements with ICP-MS. 3T3-L1 WT and *Atp7a*$^{-/-}$ cells were cultured in 100-mm dishes and treated with or without 5 μM, 25 μM, or 100 μM LA or 10 μM BCS for 24 h, 48 h, or 10 d. Cells were washed, collected into 15-mL metal-free centrifuge tubes (VWR), suspended with PBS (Gibco, cat number 14190250), and counted using the Neubauer chamber for further normalization of metal (Cu, Zn, Fe, and Mn) and Se content. Cells were pelleted, and supernatant was removed. Cell pellets were stored in −80 °C until cell digestion. Further details of sample preparations for ICP-MS are described in *SI Appendix, Supplementary Methods*.

Liquid Chromatography Coupled with ICP-MS (LC-ICP MS). 3T3-L1 WT and *Atp7a*$^{-/-}$ preadipocytes were grown on 15-cm dishes as described above. KO cells were treated with 5 or 25 μM LA for 10 d; nontreated cells were used as a control. Cells were washed and collected into clean 1.7-mL tubes. Cells were pelleted, and supernatant was removed. Cell pellets were stored in −80 °C until required. Further details of sample preparations for LC-ICP MS are described in *SI Appendix, Supplementary Methods*.

RT-qPCR. 3T3-L1 WT and *Atp7a*$^{-/-}$ cells were grown on six-well plates and treated with either 5 μM, 25 μM LA, or 10 μM BCS for 48 h or 10 d. Cells were washed and collected into clean centrifuge tubes for RNA isolation. RNA isolation and further gene expression analysis details are described in *SI Appendix, Supplementary Methods*.

Mice Husbandry and Tissue Collection. Animals were housed at the Johns Hopkins University, School of Medicine (JHU SOM) animal care facility, and the studies followed the NIH guidelines. Animal protocols were approved by the Institutional Animal Care and Use Committee (protocol number M017M385).

Atp7b KO (*Atp7b*$^{-/-}$) and WT mice of C57BL/6x129S6/SvEv background (described in ref. 45) were fed with the standard pellet chow. At 4 wk or 20 wk after birth, mice were killed and perfused with PBS (Gibco, cat number 14190250). The liver, kidney, heart, and brain were used for Cu and Se analysis. Tissues were flash-frozen and stored at −80 °C until digestion. Details of sample preparations for ICP-MS are described in *SI Appendix, Supplementary Methods*.

Live Imaging. WT and *Atp7a*$^{-/-}$ cells treated with or without 5 μM LA or 10 μM BCS for 10 d transiently expressing GRX1-roGFP were imaged with the Zeiss LSM700 or Zeiss LSM800 confocal laser scanning microscope. The sensor was excited frame by frame with a 405-nm or 488-nm laser, and emission was detected with a 505 to 600 band-pass filter. Cells were treated with 2 mM H_2O_2 or 10 mM dithiothreitol to achieve complete sensor oxidation or reduction, respectively. $IR_{405/408}$ ratios were calculated using ImageJ software. Ratiometric ($IR_{405/408}$) images were prepared with ZEN and ImageJ software after background subtraction. Generation of adenoviral constructs, adenoviral infection, and transfection for compartmentalized expression of GRX1-roGFP sensors are described in more details in *SI Appendix, Supplementary Methods*.

Seahorse XF Cell Mito Stress Test. WT and *Atp7a*$^{-/-}$ cells were plated to the 96-well Agilent Seahorse XF Cell Culture Microplate and treated with or without 5 μM LA or 10 μM BCS for 48 h. Further details are provided in *SI Appendix, Supplementary Methods*.

Analysis of Protein Oxidation State. 3T3-L1 WT and *Atp7a*$^{-/-}$ preadipocytes were cultured in 60-mm dishes and treated with 5 μM LA 10 d. Cells were washed with ice-cold PBS and collected and lysed with RIPA buffer with EDTA-free protease inhibitor cocktail on ice for 1 h and centrifuged at 3,000 *g* for 15 min. Protein concentration from the obtained lysate was estimated by the BCS assay. A mixture of 10 μg of total protein per well and 4× sample buffer were loaded to Laemmli SDS-PAGE gel and stained with Colloidal Blue staining (Thermo Fisher, LC6025) to confirm the quality of proteins. Protein lysate was further diluted to a concentration of 1 μg/μL and further prepared for the analysis.

Analysis of protein oxidation state was done using modifications to the *Pan-Protein Adductomics* approach (72), which combines nanoflow-liquid and overlapping-window data-independent acquisition, high-resolution tandem mass spectrometry. Further details on sample preparations are provided in *SI Appendix, Supplementary Methods*.

Statistical Analysis. GraphPad Prism version 9.4.1 software (GraphPad Software) was used for all statistical analysis. One-way ANOVA was used unless otherwise mentioned. All data in the figures are shown as the mean ± SD unless specified. A *P* value of less than 0.05 was considered significant.

Data, Materials, and Software Availability. All study data are included in the article and/or *SI Appendix*. All data used for generation figures in the manuscript are included with the submission (supplement). We have submitted the mass-spectrometry datasets to ProteomeXchange in PRIDE database: http://www.ebi.ac.uk/pride under identifier PXD045233 (73). The data are currently private but will become available when manuscript is published, on 9 August 2023. The data are currently private but will become available when manuscript is published.

ACKNOWLEDGMENTS. This work was supported by grants from Dora Plus 1.2 and Kristjan Jaak Scholarship Programs awarded by Archimedes Foundation (Education and Youth Board, Estonia) to E.K., NIH grants R01 DK117396 and R01 DK071865 S.L. and by the Estonian Research Council no. 1289 to (P.P.). K.S. acknowledges a postdoctoral fellowship from the Natural Sciences and Engineering Research Council of Canada. We thank Dr. Tobias P. Dick [German Cancer Research Center (DKFZ), Heidelberg, Germany] for the GRX1-roGFP2 construct. TMT-MS/MS study was performed in JHU SOM Mass Spectrometry and Proteomics Facility. We thank Dr. Tatiana Boronina and Connie Talbot for help with the proteomics result analysis and Sean M. Burke, for assistance with the Pan-Protein Adductomics data processing. ICP-MS measurements were performed in the OHSU Elemental Analysis Core with partial support from NIH (S10RR025512 and S10OD028492). Cell live imaging was performed in the Johns Hopkins MicFac facility, which was funded by the NIH grant #S10 OD016374.

Author affiliations: [a]Department of Chemistry and Biotechnology, Tallinn University of Technology, Tallinn 12618, Estonia; [b]Department of Physiology, Johns Hopkins Medical Institutes, Baltimore, MD 21205; [c]Mass Spectrometry and Proteomics Core, Johns Hopkins Medical Institutes, Baltimore, MD 21205; and [d]Department of Molecular and Medical Genetics, Oregon Health & Science University, Portland, OR 97201

1. A. K. Boal, A. C. Rosenzweig, Structural biology of copper trafficking. *Chem. Rev.* **109**, 4760–4779 (2009).
2. I. Iakovidis, I. Fau Delimaris, S. M. Piperakis, S. M. Piperakis, Copper and its complexes in medicine: A biochemical approach. *Mol. Biol. Int.* **2011**, 594529 (2011).
3. J. Arguello, D. Raimunda, T. Padilla-Benavides, Mechanisms of copper homeostasis in bacteria. *Front. Cell Infect. Microbiol.* **3**, 73 (2013).
4. A. Hordyjewska, Ł Popiołek, J. Kocot, The many "faces" of copper in medicine and treatment. *BioMetals* **27**, 611–621 (2014).
5. J. Y. Uriu-Adams, C. L. Keen, Copper, oxidative stress, and human health. *Mol. Aspects Med.* **26**, 268–298 (2005).
6. J. F. Collins, Fau Prohaska Jr., M. D. Knutson, M. D. Knutson, Metabolic crossroads of iron and copper. *Nutr. Rev.* **68**, 133–147 (2010).
7. S. Auclair *et al.*, Mild copper deficiency alters gene expression of proteins involved in iron metabolism. *Blood Cells Mol. Dis.* **36**, 15–20 (2006).
8. H. Shim, Z. L. Harris, Genetic defects in copper metabolism. *J. Nutr.* **133**, 1527S–1531S (2003).
9. J. Camakaris, J. R. Mann, D. M. Danks, Copper metabolism in mottled mouse mutants: Copper concentrations in tissues during development. *Biochem. J.* **180**, 597–604 (1979).
10. N. Shiraishi *et al.*, Metallothionein in kidney and liver of the macular mouse as an animal model of Menkes' kinky hair disease. *Physiol. Chem. Phys. Med. NMR* **19**, 227–233 (1987).
11. S. K. Das, K. Ray, Wilson's disease: An update. *Nat. Clin. Practice Neurol.* **2**, 482–493 (2006).
12. J. D. Gitlin, Wilson disease. *Gastroenterology* **125**, 1868–1877 (2003).
13. A. Gupta, S. Lutsenko, Human copper transporters: Mechanism, role in human diseases and therapeutic potential. *Future Med. Chem.* **1**, 1125–1142 (2009).
14. S. Lutsenko, N. L. Barnes, M. Y. Bartee, O. Y. Dmitriev, Function and regulation of human copper-transporting ATPases. *Physiol. Rev.* **87**, 1011–1046 (2007).
15. W.-J. Li, C. Chen, Z.-F. You, R.-M. Yang, X.-P. Wang, Current drug managements of wilson's disease: From west to east. *Curr. Neuropharmacol.* **14**, 322–325 (2016).
16. G. J. Brewer, C. A. Terry, A. M. Aisen, G. M. Hill, Worsening of neurologic syndrome in patients with wilson's disease with initial penicillamine therapy. *Arch. Neurol.* **44**, 490–493 (1987).
17. G. J. Brewer, Penicillamine should not be used as initial therapy in Wilson's disease. *Mov. Disord.* **14**, 551–554 (1999).
18. D.-B. Chen *et al.*, Penicillamine increases free copper and enhances oxidative stress in the brain of toxic milk mice. *PLOS One* **7**, e37709 (2012).
19. B. Sabine *et al.*, Bis-choline tetrathiomolybdate prevents copper-induced blood–brain barrier damage. *Life Sci. Alliance* **5**, e202101164 (2022).
20. A. Ambi *et al.*, Evaluation of copper chelation therapy in a transgenic rat model of cerebral amyloid angiopathy. *ACS Chem. Neurosci.* **14**, 378–388 (2023).
21. J. Smirnova *et al.*, Copper(I)-binding properties of de-coppering drugs for the treatment of Wilson disease. α-Lipoic acid as a potential anti-copper agent. *Sci. Rep.* **8**, 1463–1463 (2018).
22. R. L. Searls, D. R. Sanadi, α-Ketoglutaric dehydrogenase: VIII., Isolation and some properties of a flavoprotein component. *J. Biol. Chem.* **235**, 2485–2491 (1960).
23. P. Ou, H. J. Tritschler, S. P. Wolff, Thioctic (lipoic) acid: A therapeutic metal-chelating antioxidant? *Biochem. Pharmacol.* **50**, 123–126 (1995).
24. L. Packer, E. H. Witt, H. J. Tritschler, Alpha-lipoic acid as a biological antioxidant. *Free Radical Biol. Med.* **19**, 227–250 (1995).
25. X. Yi, N. Maeda, Endogenous production of lipoic acid is essential for mouse development. *Mol. Cell Biol.* **25**, 8387–8392 (2005).
26. R. Yasuno, H. Wada, The biosynthetic pathway for lipoic acid is present in plastids and mitochondria in Arabidopsis thaliana11The nucleotide sequence data of the Arabidopsis thaliana LIP1p cDNA for a lipoic acid synthase located in plastids was deposited in the DDBJ, EMBL, and GenBank nucleotide sequence databases with the accession number AB073745. *FEBS Lett.* **517**, 110–114 (2002).
27. K. P. Shay, R. F. Moreau, E. J. Smith, A. R. Smith, T. M. Hagen, Alpha-lipoic acid as a dietary supplement: Molecular mechanisms and therapeutic potential. *Biochim. Biophys. Acta* **1790**, 1149–1160 (2009).
28. M. Panigrahi *et al.*, α-Lipoic acid protects against reperfusion injury following cerebral ischemia in rats. *Brain Res.* **717**, 184–188 (1996).
29. A. Bhattacharjee *et al.*, The activity of menkes disease protein ATP7A is essential for redox balance in mitochondria. *J. Biol. Chem.* **291**, 16644–16658 (2016).
30. K.-J. Cho *et al.*, α-Lipoic acid inhibits adipocyte differentiation by regulating pro-adipogenic transcription factors via mitogen-activated protein kinase pathways*. *J. Biol. Chem.* **278**, 34823–34833 (2003).
31. M. Fernández-Galilea, P. Pérez-Matute, P. L. Prieto-Hontoria, J. A. Martinez, M. J. Moreno-Aliaga, Effects of lipoic acid on lipolysis in 3T3-L1 adipocytes. *J. Lipid Res.* **53**, 2296–2306 (2012).
32. J. R. Hahm, H. S. Noh, J. H. Ha, G. S. Roh, D. R. Kim, Alpha-lipoic acid attenuates adipocyte differentiation and lipid accumulation in 3T3-L1 cells via AMPK-dependent autophagy. *Life Sci.* **100**, 125–132 (2014).
33. S. Lutsenko, A. Gupta, J. L. Burkhead, V. Zuzel, Cellular multitasking: The dual role of human Cu-ATPases in cofactor delivery and intracellular copper balance. *Arch. Biochem. Biophys.* **476**, 22–32 (2008).
34. M. J. Petris *et al.*, Ligand-regulated transport of the menkes copper P-type ATPase efflux pump from the golgi apparatus to the plasma membrane: A novel mechanism of regulated trafficking. *EMBO J.* **15**, 6084–6095 (1996).
35. I. Bremner, Involvement of metallothionein in the hepatic metabolism of copper. *J. Nutrition* **117**, 19–29 (1987).
36. A. Krężel, W. Maret, The functions of metamorphic metallothioneins in zinc and copper metabolism. *Int. J. Mol. Sci.* **18**, 1237 (2017).

37. A. Krężel, W. Maret, The bioinorganic chemistry of mammalian metallothioneins. *Chem. Rev.* **121**, 14594–14648 (2021).
38. B. Zhang *et al.*, Activity of metal-responsive transcription factor 1 by toxic heavy metals and H2O2 in vitro is modulated by metallothionein. *Mol. Cell Biol.* **23**, 8471–8485 (2003).
39. S. Ogushi, T. Kimura, The difference in zinc concentrations required for induction among metallothionein isoforms can be explained by the different MTF1 affinities to MREs in its promoter. *Int. J. Mol. Sci.* **24**, 24010283 (2023), 10.3390/ijms24010283.
40. R. F. Burk, K. E. Hill, Regulation of selenium metabolism and transport. *Annu. Rev. Nutr.* **35**, 109–134 (2015).
41. L. Schomburg, U. Schweizer, Hierarchical regulation of selenoprotein expression and sex-specific effects of selenium. *Biochim. Biophys.* **1790**, 1453–1462 (2009).
42. B. S. Weeks, M. S. Hanna, D. Cooperstein, Dietary selenium and selenoprotein function. *Med. Sci. Monit.* **18**, RA127–RA132 (2012).
43. M. T. Howard, B. A. Carlson, C. B. Anderson, D. L. Hatfield, Translational redefinition of UGA codons is regulated by selenium availability *. *J. Biol. Chem.* **288**, 19401–19413 (2013).
44. K. A. Meacham *et al.*, Altered zinc balance in the Atp7b−/− mouse reveals a mechanism of copper toxicity in Wilson disease. *Metallomics* **10**, 1595–1606 (2018).
45. O. I. Buiakova *et al.*, Null mutation of the murine ATP7B (Wilson disease) gene results in intracellular copper accumulation and late-onset hepatic nodular transformation. *Hum. Mol. Genet.* **8**, 1665–1671 (1999).
46. A. Muchenditsi *et al.*, Systemic deletion of Atp7b modifies the hepatocytes' response to copper overload in the mouse models of Wilson disease. *Sci. Rep.* **11**, 5659 (2021).
47. S. Dev *et al.*, Oxysterol misbalance critically contributes to Wilson disease pathogenesis. *Sci. Adv.* **8**, eadc9022 (2022).
48. S. Arbogast, A. Ferreiro, Selenoproteins and protection against oxidative stress: Selenoprotein N as a novel player at the crossroads of redox signaling and calcium homeostasis. *Antioxid. Redox Signal.* **12**, 893–904 (2009).
49. Y. Zhang *et al.*, Role of selenoproteins in redox regulation of signaling and the antioxidant system: A review. *Antioxidants* **9**, 9050383 (2020), 10.3390/antiox9050383.
50. Y. Hatori *et al.*, Neuronal differentiation is associated with a redox-regulated increase of copper flow to the secretory pathway. *Nat. Commun.* **7**, 10640 (2016).
51. L. Tarrago *et al.*, The selenoprotein methionine sulfoxide reductase B1 (MSRB1). *Free Radical Biol. Med.* **191**, 228–240 (2022).
52. P. Marchetti, Q. Fovez, N. Germain, R. Khamari, J. Kluza, Mitochondrial spare respiratory capacity: Mechanisms, regulation, and significance in nontransformed and cancer cells. *FASEB J.* **34**, 13106–13124 (2020).
53. P. Tsvetkov *et al.*, Copper induces cell death by targeting lipoylated TCA cycle proteins. *Science* **375**, 1254–1261 (2022).
54. R. L. Searls, D. R. Sanadi, alpha-Ketoglutaric dehydrogenase: VIII. Isolation and some properties of a flavoprotein component. *J. Biol. Chem.* **235**, 2485–2491 (1960).
55. G. Gromadzka, A. Przybyłkowski, T. Litwin, A. Karpińska, Antioxidant capacity is decreased in wilson's disease and correlates to liver function. *Biol. Trace Element Res.* **201**, 1582–1587 (2023).
56. G. S. Mijnhout, B. J. Kollen, A. Alkhalaf, N. Kleefstra, H. J. G. Bilo, Alpha lipoic acid for symptomatic peripheral neuropathy in patients with diabetes: A meta-analysis of randomized controlled trials. *Int. J. Endocrinol.* **2012**, 456279 (2012).
57. H. Khan, T. G. Singh, R. S. Dahiya, M. M. Abdel-Daim, α-Lipoic acid, an organosulfur biomolecule a novel therapeutic agent for neurodegenerative disorders: An mechanistic perspective. *Neurochem. Res.* **47**, 1853–1864 (2022).
58. D. Ziegler *et al.*, Treatment of symptomatic diabetic polyneuropathy with the antioxidant alpha-lipoic acid: A 7-month multicenter randomized controlled trial (ALADIN III study). ALADIN III study group. Alpha-lipoic acid in diabetic neuropathy. *Diabetes Care* **22**, 1296–1301 (1999).
59. B. Salehi *et al.*, Insights on the use of α-lipoic acid for therapeutic purposes. *Biomolecules* **9**, 9080356 (2019), 10.3390/biom9080356.
60. M. T. Howard, B. A. Carlson, C. B. Anderson, D. L. Hatfield, Translational redefinition of UGA codons is regulated by selenium availability. *J. Biol. Chem.* **288**, 19401–19413 (2013).
61. R. A. Sunde, A. M. Raines, Selenium regulation of the selenoprotein and nonselenoprotein transcriptomes in rodents. *Adv. Nutr.* **2**, 138–150 (2011).
62. M. Schwarz *et al.*, Copper interferes with selenoprotein synthesis and activity. *Redox Biol.* **37**, 101746 (2020).
63. A. Dikiy *et al.*, SelT, SelW, SelH, and Rdx12: Genomics and molecular insights into the functions of selenoproteins of a novel thioredoxin-like family. *Biochemistry* **46**, 6871–6882 (2007).
64. B. R. Cardoso, B. R. Roberts, A. I. Bush, D. J. Hare, Selenium, selenoproteins and neurodegenerative diseases. *Metallomics* **7**, 1213–1228 (2015).
65. K. J. Böhm, Elevated copper ion levels as potential cause of impaired kinesin-dependent transport processes. *Arch. Toxicol.* **89**, 565–572 (2015).
66. L. Perrin *et al.*, Zinc and copper effects on stability of tubulin and actin networks in dendrites and spines of hippocampal neurons. *ACS Chem. Neurosci.* **8**, 1490–1499 (2017).
67. C. Wilson, C. González-Billault, Regulation of cytoskeletal dynamics by redox signaling and oxidative stress: Implications for neuronal development and trafficking. *Front. Cell Neurosci.* **9**, 381–381 (2015).
68. H. Cao *et al.*, Hypoxia destroys the microstructure of microtubules and causes dysfunction of endothelial cells via the PI3K/Stathmin1 pathway. *Cell Biosci.* **9**, 20 (2019).
69. R. R. Goldblum *et al.*, Oxidative stress pathogenically remodels the cardiac myocyte cytoskeleton via structural alterations to the microtubule lattice. *Dev. Cell* **56**, 2252–2266.e2256 (2021).
70. J. Sakai *et al.*, Reactive oxygen species-induced actin glutathionylation controls actin dynamics in neutrophils. *Immunity* **37**, 1037–1049 (2012).
71. L. Banci *et al.*, Affinity gradients drive copper to cellular destinations. *Nature* **465**, 645–648 (2010).
72. J. W. Smith *et al.*, Global discovery and temporal changes of human albumin modifications by pan-protein adductomics: Initial application to air pollution exposure. *J. Am. Soc. Mass Spectrom.* **34**, 595–607 (2023).
73. E. Kabin *et al.*, α-Lipoic acid ameliorates consequences of copper overload by 6 upregulating selenoproteins and decreasing redox misbalance. PRIDE Archive. https://www.ebi.ac.uk/pride/. Deposited 8 September 2023.